



Kent Academic Repository

Marques, M.J., Green, Robert, King, Roberto, Clement, Simon, Hallett, Peter and Podoleanu, Adrian G.H. (2020) *Sub-surface characterisation of latest-generation identification documents using optical coherence tomography*. Science and Justice . ISSN 1355-0306.

Downloaded from

<https://kar.kent.ac.uk/85229/> The University of Kent's Academic Repository KAR

The version of record is available from

<https://doi.org/10.1016/j.scijus.2020.12.001>

This document version

Author's Accepted Manuscript

DOI for this version

Licence for this version

CC BY-NC-ND (Attribution-NonCommercial-NoDerivatives)

Additional information

Versions of research works

Versions of Record

If this version is the version of record, it is the same as the published version available on the publisher's web site. Cite as the published version.

Author Accepted Manuscripts

If this document is identified as the Author Accepted Manuscript it is the version after peer review but before type setting, copy editing or publisher branding. Cite as Surname, Initial. (Year) 'Title of article'. To be published in *Title of Journal*, Volume and issue numbers [peer-reviewed accepted version]. Available at: DOI or URL (Accessed: date).

Enquiries

If you have questions about this document contact ResearchSupport@kent.ac.uk. Please include the URL of the record in KAR. If you believe that your, or a third party's rights have been compromised through this document please see our [Take Down policy](https://www.kent.ac.uk/guides/kar-the-kent-academic-repository#policies) (available from <https://www.kent.ac.uk/guides/kar-the-kent-academic-repository#policies>).

Journal Pre-proofs

Sub-surface characterisation of latest-generation identification documents using optical coherence tomography

Manuel J. Marques, Robert Green, Roberto King, Simon Clement, Peter Hallett, Adrian Podoleanu

PII: S1355-0306(20)30333-6
DOI: <https://doi.org/10.1016/j.scijus.2020.12.001>
Reference: SCIJUS 924

To appear in: *Science & Justice*

Received Date: 7 August 2020
Revised Date: 19 November 2020
Accepted Date: 21 December 2020

Please cite this article as: M.J. Marques, R. Green, R. King, S. Clement, P. Hallett, A. Podoleanu, Sub-surface characterisation of latest-generation identification documents using optical coherence tomography, *Science & Justice* (2020), doi: <https://doi.org/10.1016/j.scijus.2020.12.001>

This is a PDF file of an article that has undergone enhancements after acceptance, such as the addition of a cover page and metadata, and formatting for readability, but it is not yet the definitive version of record. This version will undergo additional copyediting, typesetting and review before it is published in its final form, but we are providing this version to give early visibility of the article. Please note that, during the production process, errors may be discovered which could affect the content, and all legal disclaimers that apply to the journal pertain.

© 2020 Published by Elsevier B.V. on behalf of The Chartered Society of Forensic Sciences.



Sub-surface characterisation of latest-generation identification documents using optical coherence tomography

Manuel J. Marques^{1,*†}, Robert Green^{2,†}, Roberto King³, Simon Clement³,
Peter Hallett³, and Adrian Podoleanu¹

¹*Applied Optics Group, School of Physical Sciences, University of Kent, Canterbury CT2 7NH, United Kingdom.*

²*Forensic Research Group, School of Physical Sciences, University of Kent, Canterbury CT2 7NH, United Kingdom*

³*Foster and Freeman Ltd, Vale Park, 2 Vale Link, Evesham WR11 1TD, United Kingdom*

*Corresponding author: M.J.Marques@kent.ac.uk

†Both authors have contributed equally to the manuscript.

Disclosures

A. Podoleanu: patents owned by the University of Kent on the Master Slave OCT technology employed in the paper.

Acknowledgements

The authors acknowledge the support of Foster and Freeman, Ltd. in supplying a specimen passport to be analysed in this study, and in particular Bob Dartnell, Tom McCotter and David Tobin. M. J. Marques, R. Green and A. Podoleanu acknowledge financial support from the School of Physical Sciences, University of Kent, which enabled the interaction with Foster and Freeman. M. J. Marques and A. Podoleanu also acknowledge the following sources of funding: Biotechnology and Biological Sciences Research Council (BBSRC) (*5DHiResE* project, grant number BB/S016643/1) and the Engineering and Physical Sciences Research Council (EPSRC) (*REBOT* project, grant number EP/N019229/1 and EP/N027078/2). A. Podoleanu also acknowledges support from the National Institute for Health Research (NIHR) Biomedical Research Centre at the UCL Institute of Ophthalmology, University College London, the Moorfields Eye Hospital NHS Foundation Trust, and the Royal Society Wolfson research merit award.

ABSTRACT

The identification of individuals, particularly at international border crossings, coupled with the evolving sophistication of identity documents are issues that authorities must contend with. Particularly, the ability to distinguish legitimate from counterfeit documents, with high throughput, sensitivity, and selectivity is an ever-evolving challenge.

Over the last decade, an increasing number of security features have been introduced by authorities in identification documents. The latest generation of travel documents (such as passports and national ID cards) forego paper substrates for several layers of polycarbonate, allowing security features to be embedded within the documents. These security features may contain information at either the superficial and sub-surface levels, thus increasing the document's resilience to counterfeiting.

As the documents become harder to forge, so does the sophistication of forgery detection. There appears to be an unmet and evolving need to identify such sophisticated forgeries, in a non-destructive, high throughput manner.

In this publication, we report on the application of optical coherence tomography (OCT) imaging on assessing security features in specimen passports and national ID cards. OCT allows sub-surface imaging of translucent structures, non-destructively enabling quantitative visualisation of embedded security features.

1. Introduction

The identification of individuals, especially at international border crossings, has always been an issue that authorities must contend with. In particular, the ability to distinguish legitimate from counterfeit identification documents, and to do so quickly and with high sensitivity and selectivity are recurring challenges. Experts within law enforcement and border security cite passport fraud as the greatest threat to global security [1]; such are the significance and consequences where technology falls behind criminals, who would seek to exploit identity documents for illegitimate travel or money laundering purposes.

The UK government point out and acknowledges the large number of fraudulent identity documents in circulation [2] and continue to invest in the field of identification document validation technology. A review of contemporary literature [2–6] point towards a large-scale crime problem linked with organised, transnational crime and raising the threat of criminals and terrorists crossing borders undetected. A considerable body of knowledge suggests that in order to provide high levels of security, the document should combine a number of different, multifunctional features [8].

While significant advances have been made to ensure that these documents are not easily forged or altered, it is important that we stay one step ahead of the criminals and forgers. Hence, Governments are regularly refining production methods to add levels of security. The manufacturing of these documents has become ever more sophisticated, with a range of

security features making counterfeiting ever more difficult. As the design of these documents becomes ever more complex the greater the challenges in detecting forgeries becomes, and consequently an increased need for more complex forensic technologies to uncover such counterfeits.

These technologies are introduced in response to the identified needs of law enforcement, and their level of complexity range from the simple, manual check at one extreme and increase in line with the levels of assurance needed for those checks associated with employment or access to critical infrastructure. At the simplest level, the examination of these (and other) documents can be achieved by both simple and complex optical imaging systems employing a wide wavelength range of polarised and oblique light sources [9,10], coupled with computer-based pattern detection and comparison [11]. Without seeking to give a lower profile to the other methods used to detect counterfeit identity documents [12], the prevailing need within contemporary forensic investigation may be categorised as: speed of analysis; straightforward and easily understood applications and non-destructive testing. Among the more sophisticated, deployable technologies is the video spectral comparator (VSC) [13]. The VSC can differentiate between genuine and counterfeit documents using a combination of transmitted, direct or oblique light, incorporating light sources with wavelengths of radiation spanning the ultraviolet to the infrared regions of the electromagnetic spectrum. This equipment is widely used to differentiate between inks, reveal alterations and most importantly to visualise security features in documents as well as examining the characteristics of hologram, watermark features, and fibre disturbance in documents [14]. Similarly, techniques of passport examination by confocal type laser profile microscopes have been suggested focusing particularly upon the thickness of the polycarbonate film layer [9].

Since the launch of the machine-readable passports, circa 1980s, the manufacture and design of identification documents have gone through several iterations. The latest generation of identification documents are manufactured by fusing together several semi-transparent layers of varying thicknesses, each of them containing different security features and/or information, producing a final, single-page, document. In this manner, the security features are distributed not just in different superficial areas of the document, but also located along several sub-superficial depths.

Each technical development increases the resistance to fraud but despite this, the threats posed by fraudsters in 2020 are both widespread and serious [8]. Although, undoubtedly more secure than their predecessors, the latest generation of identity documents manufactured using polycarbonate layers remain susceptible to counterfeiting. Amongst the tactics used by fraudsters are the copying of paper or polycarbonate, reproducing the documents using

sophisticated computer technology, reproducing hologram images and re-laminating. Any of these tactics will affect the inner structure of the document, showing the importance of its sub-surface characterisation.

Sub-surface imaging would address several points: (i) by assessing the depths at which each layer is placed, and comparing their depth values against a 'ground truth' (supplied by the manufacturer), we would be able to assess whether tampering or forgery has occurred; (ii) if there is evidence of the latter, one might be able to retrieve evidence from the document itself (for instance, fingermarks embedded into the laminates); (iii) aid in quality control processes employed by the manufacturers of identification documents themselves.

Based on our experience and a review of the available literature, one technique which shows significant potential for sub-surface characterisation of documents is optical coherence tomography (OCT). Since its debut in 1991 [15], OCT imaging has been widely used in the medical and biomedical fields, recognised as transforming the field of clinical ophthalmology [16]. This technique [17] relies on the principle of low-coherence interferometry to depth profile scattering samples, with a resolution of tens of microns and over a range of a few millimetres (sample-dependent). By coupling the low-coherence interferometry with a 2-D beam-scanning system (such as a pair of galvanometric scanners) it is possible to obtain a 3-D volume of the object being studied, non-invasively and non-destructively. Given its potential for non-destructive imaging applications beyond the biomedical field, OCT imaging has found uses in several aspects of forensic sciences, including forensic anthropology, forensic medicine, and entomology [16], including blood stain imaging [18] and reconstruction of tattoos in decomposed skin tissue [19]. We also note reports of OCT in the field of banknote authentication [10,20], automotive paint characterisation [21,22] and art fraud – with even the potential for creating authenticity databases [23]. Moreover, owing to its non-destructive nature, considerable interest has been devoted to the use of OCT imaging in detection of latent fingermarks in translucent substrates [24–27]; given the near real-time aspect of this imaging technique, there have also been reports on using OCT imaging as a reliable anti-spoof fingerprint authentication method [28,29]. These examples and more would, we feel, benefit the forensic science community as a whole and, in particular, the field of document authentication.

In this publication, we aim to apply OCT imaging specifically to a structural assessment of the latest-generation of identification documents, such as passports and national ID cards. These documents possess sub-surface security features. OCT will be able to accurately reveal the separate polycarbonate layers for both passports and identity cards in real-time and non-destructively. Our research would point towards the benefits of OCT in the detection of

sophisticated counterfeits and also by the introduction of OCT-readable features during the manufacture of identity documents.

2. Materials and Methods

The OCT imaging system used in this study is a custom-built swept-source-based system, similar to the one reported by Marques *et al.* [30]. The optical source (Axsun OCT engine) emits light in the near infra-red, with an imaging wavelength of $1.06\ \mu\text{m}$, allowing acquisition of a dense volume ($500 \times 500 \times 500$ pixels, covering up to $12 \times 12 \times 6\ \text{mm}^3$) in roughly 5 seconds, with an axial resolution of $\sim 10\ \mu\text{m}$, and a lateral resolution of $\sim 15\ \mu\text{m}$.

In the sub-sections that follow, a brief explanation of the working principle of OCT is presented, along with the different manners the acquired data is processed and represented.

2.1. Anatomy of an optical coherence tomography system

Optical coherence tomography (OCT) imaging is based upon the principle of low-coherence interferometry, coupled with a scan head which allows the beam to probe the sample under examination in the two orthogonal directions to the beam propagation. A schematic representation of an OCT system like the one employed in this study is shown in Figure 1.

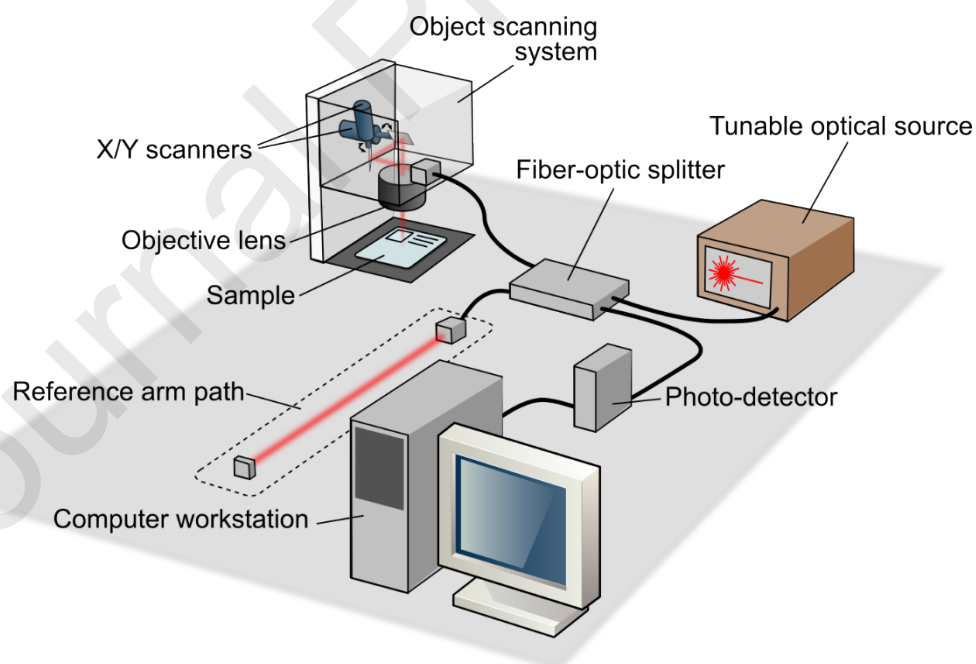


Figure 1. Simplified schematic diagram of the swept-source OCT system employed in this study.

Light from a tuneable laser, with a broad tuning range, is split between two paths: one of a known length, the reference path, and one containing the sample under study, the object path. In the reference path, light is reflected back from a mirror placed at its end; in the path leading

to the sample, light is focused into the sample, and it can either be back-reflected specularly (due to changes in the index of refraction) or backscattered by the inner structure of the sample. After light returns from both paths, it is then recombined, and the resulting optical signal is detected by a photodetector unit. The sketch aimed to reduce the complexity of the optics employed, details are in [30], where the reference is recirculated, two splitters are used, and the photodetector unit consists in two photodetectors in a balance detection scheme.

Since the optical source varies its output wavelength constantly over time (at 100 kHz), a time-resolved optical signal detected by the photo-detector unit will equate to the source's optical spectrum, with frequency modulations on top of it caused by the returned light from under (and from) the sample surface interfering with the light returning from the reference path.

These modulation frequencies are proportional to how deep light has penetrated into the sample, therefore, it is possible to reconstruct a 1-D depth profile of the sample, up to a few millimetres (albeit this may vary depending on the kind of sample being investigated).

In order to characterise the sample in the other two physical dimensions, the beam of light probing the sample is steered using a set of X/Y scanners (Figure 1, top left) in conjunction with an objective lens focusing the beam into the sample, thus allowing the system to raster-scan it.

By combining the two lateral scanned directions with the demodulation of the optical spectra detected, it is possible to obtain full three-dimensional representations of the sample under study.

2.2. OCT image rendering

Depending on the raster scan pattern employed, and how the data is processed, it is possible to obtain and represent images across different planes within the imaged volume.

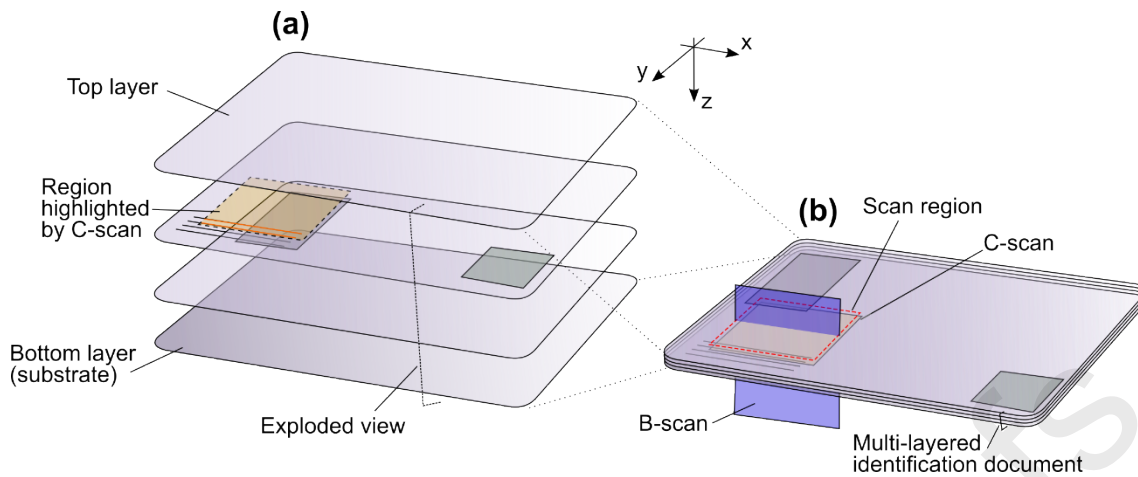


Figure 2. Application of different OCT orthogonal slicing capabilities to a multi-layered identification document. **(a)** exploded view of identification document in **(b)**. Sub-diagram **(b)** also shows the different imaging planes which can be rendered using OCT imaging

Figure 2 illustrates the capabilities of the instrument in imaging slices along orthogonal directions in a modern identification document, equipped with security features/biographical details at different depths.

The red dashed section in Figure 2 (b) depicts the region scanned over by the X/Y scanners. It is possible to obtain constant-depth slices (termed “C-scans” in OCT literature), such as the orange shaded region present in both sub-figures of Figure 2.

It is also possible to have depth maps by fixing one of the lateral directions and constructing a X/Z or Y/Z image, which are termed “B-scans” in OCT literature, as shown in Figure 2 (b).

To render all these images, the optical spectra are demodulated, so that the individual depths can be resolved. In conventional OCT processing, this demodulation operation is typically achieved by inverse Fourier transforming the spectral information (utilising a Fast Fourier Transform (FFT) algorithm). However, before this operation can take place, it is necessary to ensure that the spectral information is sampled in the correct domain [31,32], as the depth z and the wavenumber k are Fourier pairs, but the spectral information is typically acquired in the wavelength λ domain, where $\lambda = 2\pi/k$; some other signal conditioning may be necessary, such as compensating for any dispersion mismatches caused by different optical materials present in either path of the interferometer [33]. Not only this introduce additional complexity in the system, but it can also adversely affect the performance of the instrument (namely, the imaging rate).

The Complex Master-Slave OCT (CMS-OCT) processing, pioneered by our group [34,35], addresses the issues presented above by carrying out the spectral processing in a slightly different manner. Instead of Fourier transforming each individual spectra following all necessary signal conditioning operation, CMS-OCT demodulation relies on a comparison

operation between the spectra arriving from the sample and a set of pre-generated/captured spectra (called “masks” in our previous publications) representing all possible distinct axial positions that the system is capable of imaging.

Due to its operating principle, it is easier to achieve direct C-scan image rendering with CMS-OCT, by performing the comparison operation against a single “mask”, which is particularly useful when imaging planar samples containing different features placed at each constant depth plane, which is effectively the structure of most modern identity documents.

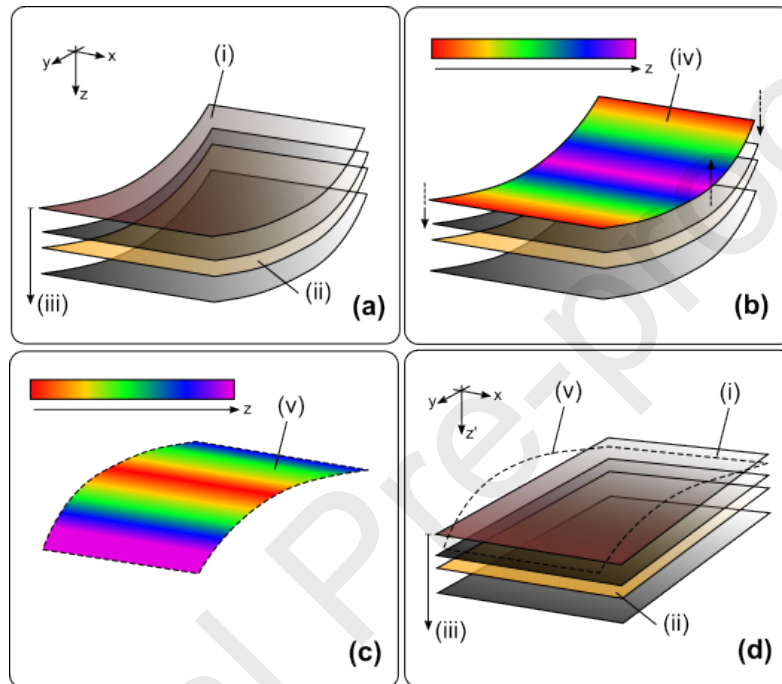


Figure 3. Procedure for virtually flattening curved/tilted documents with CMS-OCT. **(a)** the curved/tilted document as retrieved from the reconstructed OCT volume, with (i) being the document surface, (ii) being the layer of interest, and (iii) the depth coordinate below the surface. **(b)** surface detection and depth-mapping (colour-coded (iv)); **(c)** a curvature correction map (v) is constructed from the surface map (iv); **(d)** all the planes below the surface (i) are flattened by means of the curvature correction map (v), allowing full reconstruction of layer (ii).

With CMS-OCT, it is also possible to virtually “flatten” curved documents by synthesising a x,y distribution of masks which follow the top surface. Not only will this allow compensating for the inherent curvature of the imaged region (which becomes particularly critical when large scanning areas are considered, due to the limitations of the imaging objective), but in some cases it might actually be beneficial to have the document slightly tilted, to avoid saturating the photo-detector with strong specular back-reflections from the first surface of the document.

This procedure, shown schematically in Figure 3, is achieved by detecting the first surface of the volume, (i), (which can be done by a simple thresholding operation), and isolating the corresponding masks, thus creating a 2-D x,y surface height distribution, (iv) (which is colour-coded, as shown in Figure 3 (b)), with each point associated with the mask which in turn

corresponds to the height of the surface layer at that local (x,y) point, generating the curvature correction map (v) . Afterwards, any C-scans constructed will be generated from a sub-set of masks, taking into consideration the relative depth (iii) to the surface layer (i), yielding a flattened volume, as shown in (d). Effectively, the depth coordinate z is transformed into a relative depth coordinate z' (relative to the surface map (v)), with a dependency on the lateral coordinates (x,y) .

3. Results and Discussion

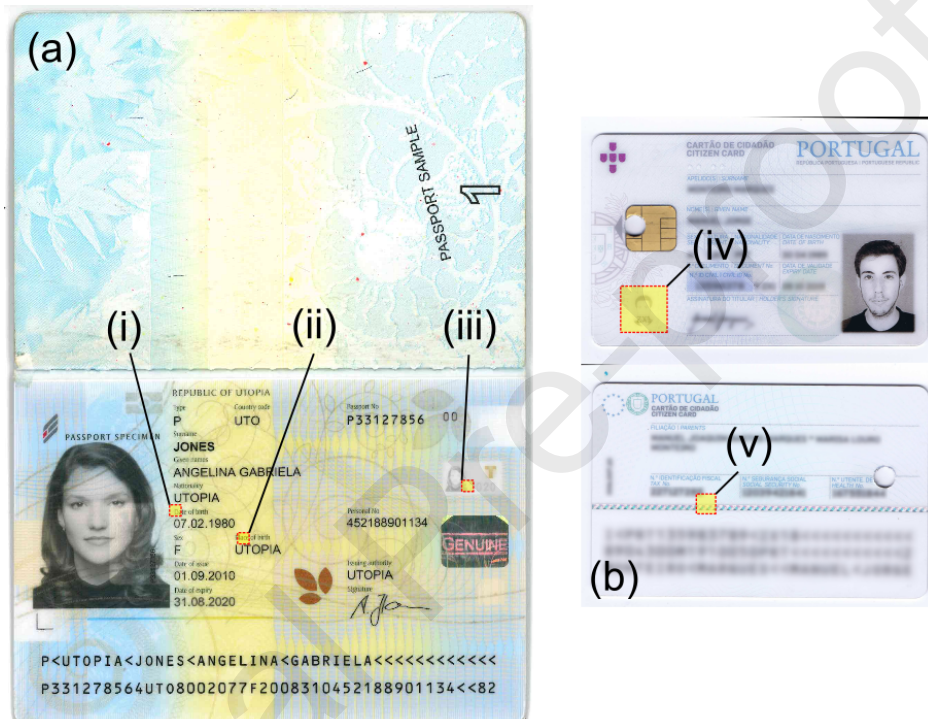


Figure 4. Documents analysed in this study. (a) specimen polycarbonate passport; (b) expired Portuguese national ID card. (i) to (v) correspond to the imaged regions in each document, to be presented throughout this section.

In order to illustrate the practical utility of our OCT system for forensic document examination, we have investigated two distinct documents: a modern polycarbonate specimen passport, supplied by Trüb AG (Switzerland), and a national identification (ID) card (expired), issued by the Portuguese Government (manufactured by *Imprensa Nacional Casa da Moeda* [36]). Full colour photographs of both documents are shown in Figure 4.

Due to the small lateral scan range of the system (up to $12 \times 12 \text{ mm}^2$), we have taken a number of small-scale volumes over both documents, labelled (i)-(v) in Figure 4; (i)-(iii) refer to different positions over the biographical page of the polycarbonate passport, and (iv)-(v) to two security features taken in the front and back of the national ID card, respectively.

3.1. Polycarbonate passport biographical page

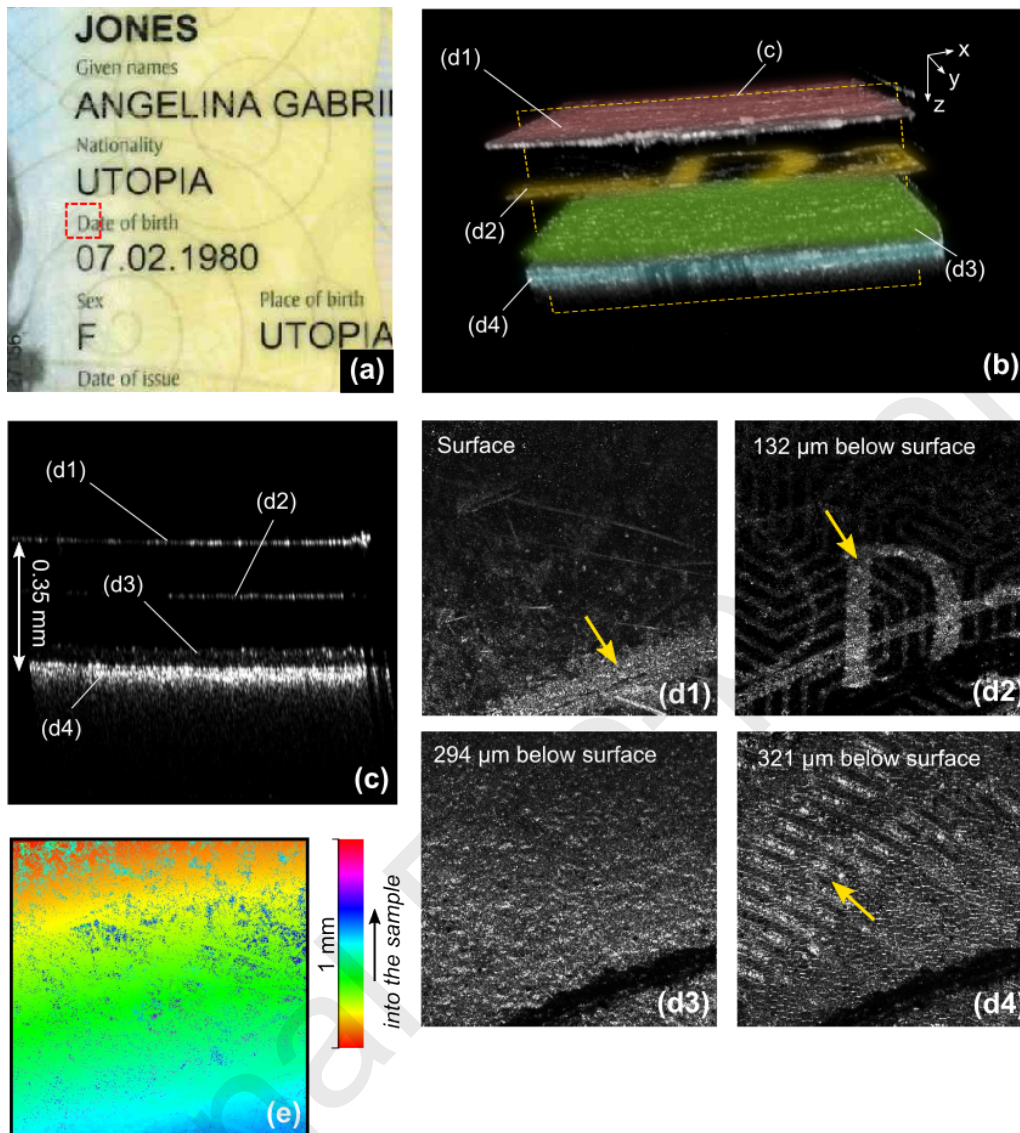


Figure 5. Volume (i) from the specimen passport. **(a)** close-up of the full-colour photograph showing the scanned region (red dashed square); **(b)** 3-D render of the reconstructed OCT volume, with depth-dependent colour-coding; **(c)** B-scan taken along the middle of the volume (dashed region in (b)); **(d1)-(d4)** C-scans covering different depths below the surface of the document, yellow arrows correspond to features mentioned in the text; **(e)** colour-coded surface map, used to flatten the C-scans in (d1)-(d4). Lateral scanned area is $2 \times 2 \text{ mm}^2$.

Images obtained from the volume (i) in Figure 4 are shown in Figure 5. The scanned region intersects the label for the “Date of birth” field in the biographical page of the passport, with the first two characters being visible in both the 3-D volume reconstruction (b), and one of the C-scan images (d2). It is possible to discern four separate layers in this region of interest, as shown colour-coded in the 3-D volume reconstruction (b). By taking a B-scan across the volume (c), the measured region spans roughly 0.35 mm in depth from the surface of the document, (d1).

The aforementioned four separate layers, shown in (d1)-(d4), include the surface of the document itself (d1), with an embossed feature, which is part of the larger spiral seen in (a), and a number of surface scratches, which were also picked up by the surface map (e). The actual printed characters “Da” are part of a layer (d2) which is roughly $132\ \mu\text{m}$ below the surface. Further below this layer, one can appreciate a textured layer (d3) which then gives rise to a patterned layer (d4). This last layer, however, seems to only be present in half of the region considered; according to (a), the region considered has a non-uniform background, (with a gradient), hence, this is not totally unexpected. Due to its high scattering properties, the embossed feature seen in (d1) produces a shadow visible in all layers below it.

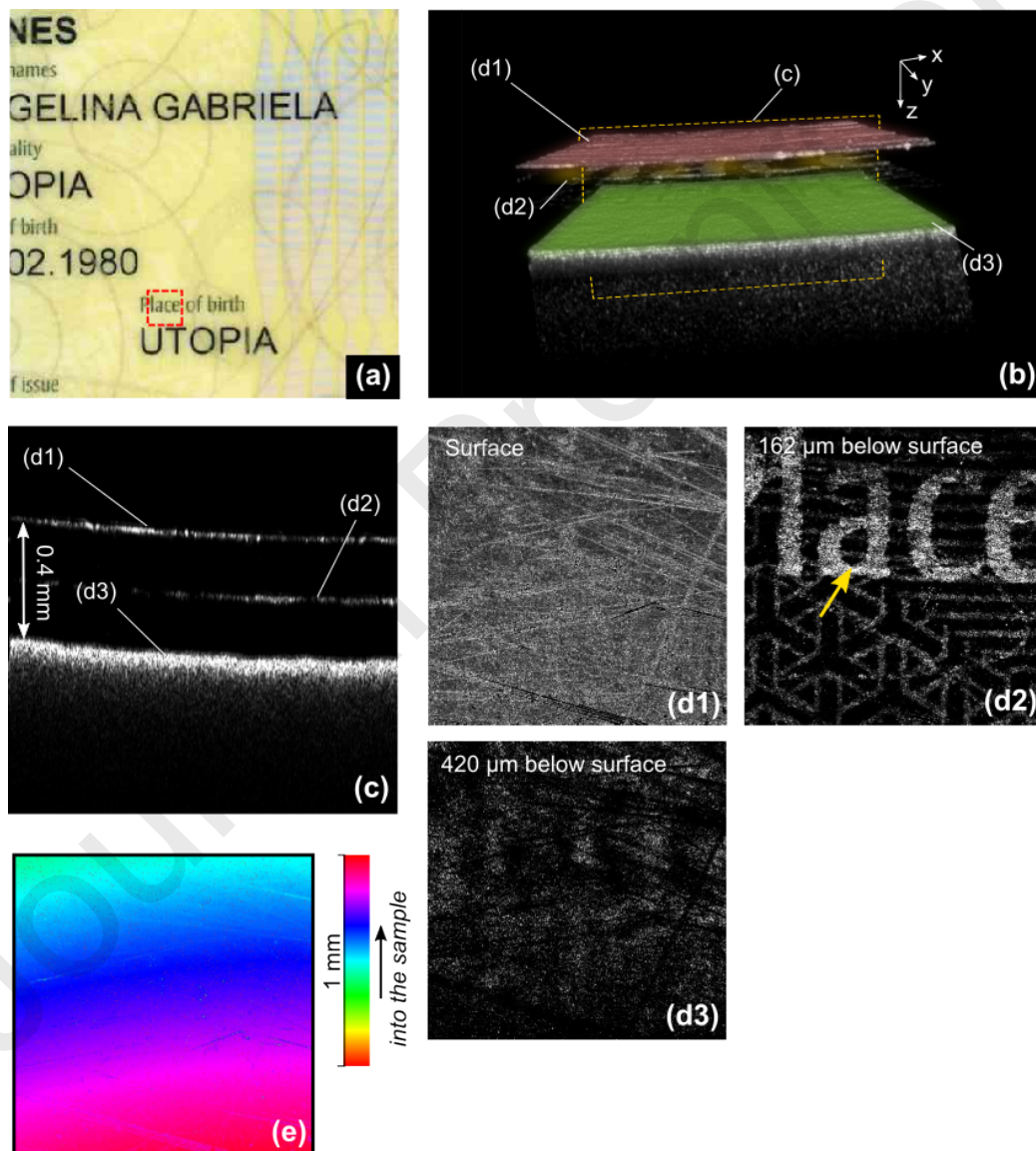


Figure 6. Volume (ii) from the specimen passport. **(a)** close-up of the full-colour photograph showing the scanned region (red dashed square); **(b)** 3-D render of the reconstructed OCT volume, with depth-dependent colour-coding; **(c)** B-scan taken along the middle of the volume (dashed region in (b)); **(d1)-(d3)** C-scans covering different depths below the surface of the document, yellow arrows correspond to features mentioned in the text; **(e)** colour-coded surface map, used to flatten the C-scans in (d1)-(d3). Lateral scanned area is $2 \times 2\ \text{mm}^2$.

Volume (ii), as shown in Figure 6, was collected from a different region of the biographical page. In this case, the background is more uniform, and there are no embossed features in the surface. The thickness of the transparent layers above the polycarbonate substrate is similar to volume (i) (around 0.35-0.4 mm), with the layer containing the printed characters being 162 μm below the surface.

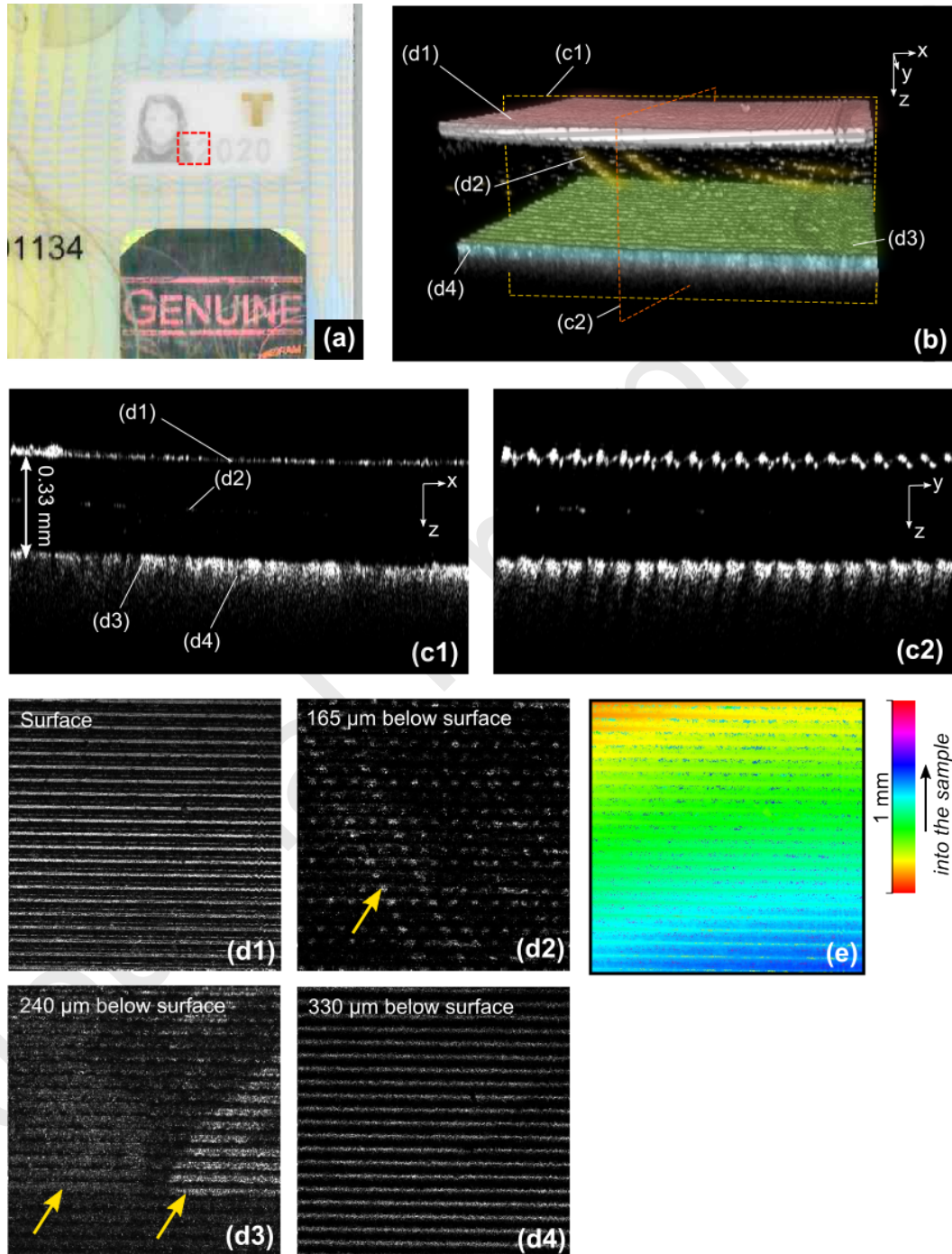


Figure 7. Volume (iii) from the specimen passport. **(a)** close-up of the full-colour photograph showing the scanned region (red dashed square); **(b)** 3-D render of the reconstructed OCT volume, with depth-dependent colour-coding; **(c1)-(c2)** B-scans taken along the middle of the volume over the two orthogonal directions (dashed regions in (b)); **(d1)-(d4)** C-scans covering different depths below the

surface of the document, yellow arrows correspond to features mentioned in the text; **(e)** colour-coded surface map, used to flatten the C-scans in (d1)-(d4). Lateral scanned area is $2 \times 2 \text{ mm}^2$.

The final volume (iii) acquired from the specimen passport (main results in Figure 7) covers an optical-based security device, a kinegram. The region covered by the scanning beam intersects the right shoulder of the person depicted in the photograph, along with a portion of the number “2”, as shown in (a).

The surface presents a regular sawtooth-like structure, which is also visible in the surface map (e). This structure repeats itself along the y direction, as evidenced by the B-scan (c2).

There are two separate patterns in this security feature, one located at $165 \mu\text{m}$ below the surface, (d2), which contains a pair of diagonal lines, and another at $240 \mu\text{m}$, containing the aforementioned portion of the person’s photograph and the number “2”, both of which are visible in the colour photograph.

Similarly, to what was observed in volume (i), the surface elements are highly scattering, producing shadows which can be seen across all C-scans below the one corresponding to the surface, (d1).

3.2. National ID card

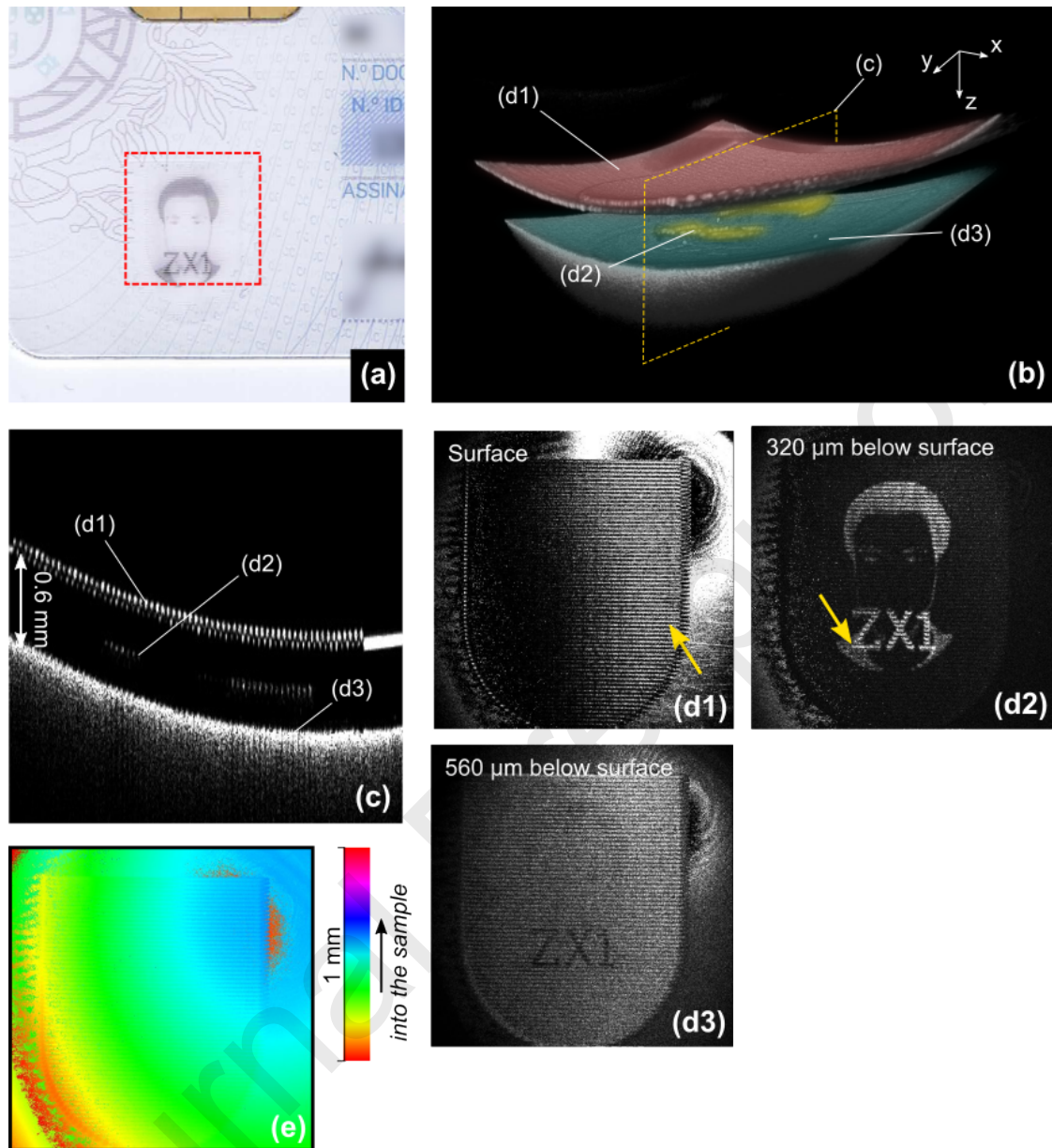


Figure 8. Volume (iv) from national ID card. **(a)** close-up of the full-colour photograph showing the scanned region (red dashed square); **(b)** 3-D render of the reconstructed OCT volume, with depth-dependent colour-coding; **(c)** B-scan taken along the middle of the volume (dashed region in (b)); **(d1)-(d3)** C-scans covering different depths below the surface of the document, yellow arrows correspond to features mentioned in the text; **(e)** colour-coded surface map, used to flatten the C-scans in (d1)-(d3). Lateral scanned area is $10 \times 10 \text{ mm}^2$.

In the front of this card, across its lower-left corner, there is a kinegram, similar to the one present in volume (iii). In this case, the security feature contains a thresholded version of the document holder's photograph, along with a control digit. Figure 8 presents the results from volume (iv), covering the kinegram. The layer containing the thresholded photograph and control digits is located $320 \mu\text{m}$ below the document surface. Again, due to the surface roughness, and high scattering present in layer (d2), some shadowing artefacts are present

in the lower layers, namely in (d3), where we should expect to see the plastic substrate of the card as a relatively uniform surface.

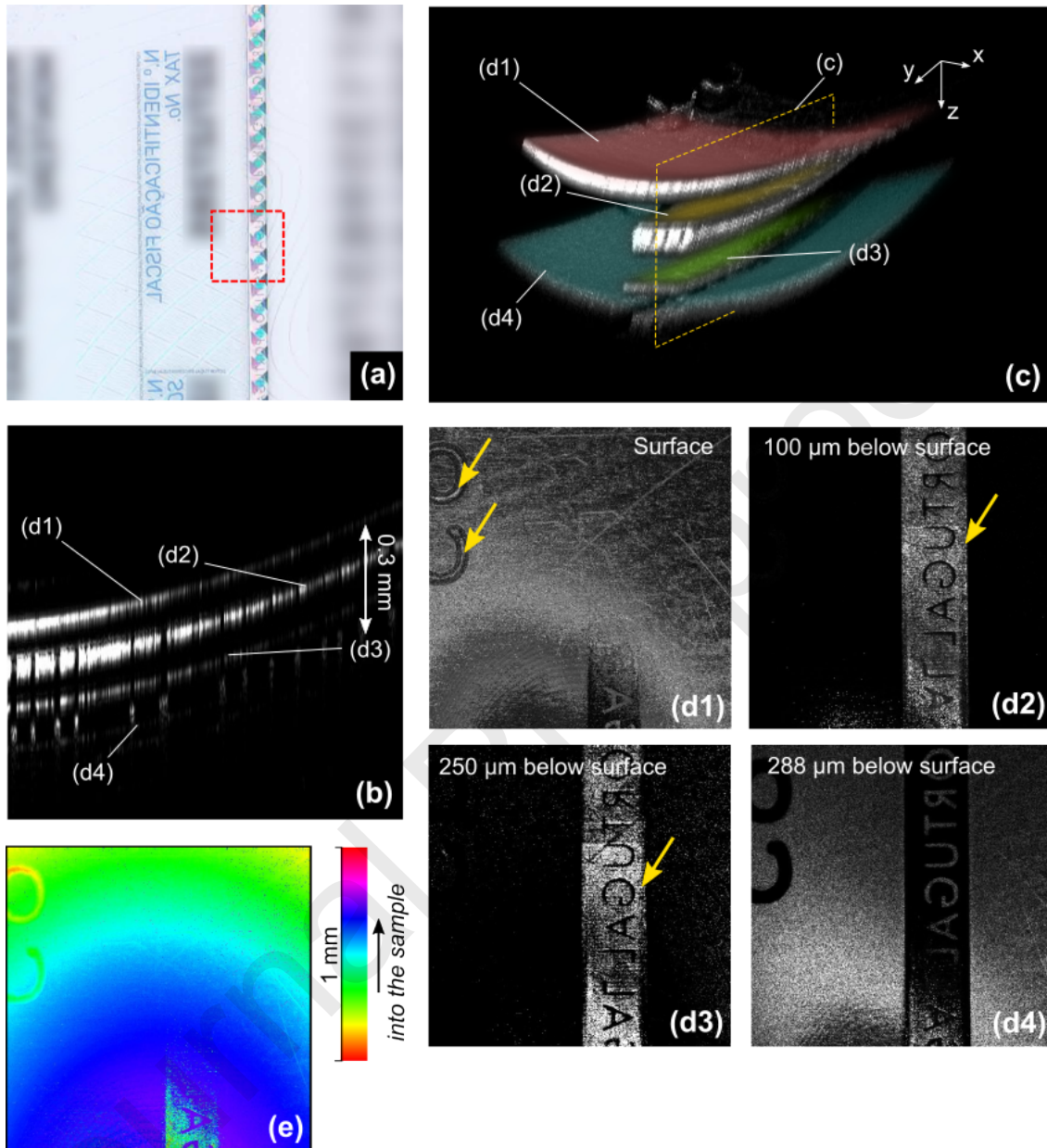


Figure 9. Volume (v) from national ID card. **(a)** close-up of the full-colour photograph showing the scanned region (red dashed square); **(b)** 3-D render of the reconstructed OCT volume, with depth-dependent colour-coding; **(c)** B-scan taken along the middle of the volume (dashed region in (b)); **(d1)-(d4)** C-scans at different depths below the surface of the document, yellow arrows correspond to features mentioned in the text; **(e)** colour-coded height map, used to axially shift the sets of masks relatively to each other from one lateral pixel to the next, leading to flattening the C-scans in (d1)-(d4). Lateral scanned area is $5 \times 5 \text{ mm}^2$.

The last sample volume investigated in this study is represented in Figure 9. Volume (v) from national ID card. **(a)** close-up of the full-colour photograph showing the scanned region (red dashed square); **(b)** 3-D render of the reconstructed OCT volume, with depth-dependent colour-coding; **(c)** B-scan taken along the middle of the volume (dashed region in

(b)); **(d1)-(d4)** C-scans at different depths below the surface of the document, yellow arrows correspond to features mentioned in the text; **(e)** colour-coded height map, used to axially shift the sets of masks relatively to each other from one lateral pixel to the next, leading to flattening the C-scans in (d1)-(d4). Lateral scanned area is 5 x 5 mm². Along the back of the card, there is a stripe containing a multi-layered hologram; volume (v) intersected part of this hologram, along with part of two digits from the national tax number, embossed on the card.

The hologram is split into several layers, ranging from 100 to 288 μm below the document surface. It is interesting to note that the hologram is placed below the transparent cover material, i.e., not actually flush with the surface.

Due to the hologram being mainly composed of metal films, some shadowing is observed in the deeper layers, since light will be specularly reflected from the shallower layers.

4. Conclusions

The results presented demonstrate that OCT can perform quantitative, non-destructive, high-resolution sub-surface analysis of multi-layered identification documents. The imaging throughput is also quite high, with a high-density volume (500x500 lateral points) typically taking less than 10 seconds to acquire, and with the CMS-OCT procedure allowing for direct visualisation of C-scan images, it is possible to obtain immediate virtual slices of the document under study. While a certain degree of depth selection would also be possible when employing a confocal microscope (whilst retaining the non-destructive nature of the technique), to achieve the same order of magnitude in terms of axial resolution of the OCT system presented here ($\sim 10 \mu\text{m}$), one would require a much higher numerical aperture objective (over 0.3), which would then sacrifice lateral range, and would require placing the sample very close to the imaging optics. Moreover, due to its interferometric principle, OCT is more sensitive than confocal microscopy, as the weak signal from the sample is multiplied with a stronger reference wave to enable interference. This enhanced sensitivity reflects in deeper penetration into the document.

Inherently a non-destructive imaging method, OCT can preserve evidence which may be useful for a criminal investigation, or, on the other hand, prevent destruction of legitimate documents which may have been previously flagged as suspected forgeries. Our review of the literature has identified some application of OCT to target forensic science problems we feel these are inconsiderable when compared against the great, yet underutilised potential of the interferometric imaging technique of OCT in a range of forensic applications. Taking into consideration some of the published reports on latent fingerprint detection with OCT imaging [24–27], we conjecture it should be possible to virtually “lift” fingerprints that may have been

left behind in the laminates of forged documents, without physically destroying the evidence in question.

OCT can also be integrated with other imaging modalities, such as fluorescence imaging [37], or photo-acoustic imaging [38,39], the spectroscopic variant of the latter allowing for the detection of specific chemical profiles.

Depth penetration into laminates of up to 0.5 mm is demonstrated in this study. Achieving longer imaging depths will depend on several factors: (i) the sample being imaged, as if the scattering coefficient is too high, or the sample is too absorbing, not enough light will reach the deeper layers (creating the shadowing artefacts visible in some of the results in Section 3); (ii) the wavelength of the light used, as longer wavelengths (into the mid-infrared, above 1.5 μm) tend to be scattered less, and therefore light will penetrate further into the structure. OCT systems in the mid-IR region have been reported [40–42]; due to a combination of reduced imaging applications at these wavelengths (increased water absorption for wavelengths $> 1.3 \mu\text{m}$ render these systems unsuitable for any biomedical imaging applications) and technical limitations in terms of photo-detection hardware, they are not as widespread and developed as their shorter wavelength counterparts.

Newer electronic (e-)passports introduce an additional and perhaps less easily imitated security feature, in the form of embedded mini-controller RFID chips which store more personal data than that listed in the biographical page, along with other secure details. Beyond e-passports, the UK biometric residence permit (BRP), issued by the Home Office to non-EU nationals, also share several security features with electronic passport – namely polycarbonate body and the mini-controller which securely stores ID data; this type of identification card is expected to be rolled out to all European Union citizens across the EU-27 by mid-2021 [43]. Unlike passports, these identity documents are often opaque and perhaps not ideally suited to traditional optical methods of identification. In this sense, mid-IR OCT systems may be useful to locate and characterise embedded mini controllers, as demonstrated by Israelsen *et al.* [40], where a contactless debit card chip was imaged non-destructively at an imaging wavelength of 4 μm .

It is important to note that all distance measurements in the axial direction are done in respect to a reference path, which has been implemented in air, with a refractive index of 1. Since the materials composing the multi-layered identification documents under study tend to have refractive indices larger than 1, to obtain the “real” physical distances, one will need to know the refractive indices of the materials, or determine them via an alternate method, such as refractometry. While this may seem to be a very significant limitation of the technique, it effectively provides an additional layer of security, as only the document manufacturer can

supply the exact information concerning the materials employed in the construction of the document, which includes the refractive indices of the materials.

The typically small lateral scan area (up to 12x12 mm² with the system presented here, but requiring more time when covering larger areas due to more pixels being needed) presents a limitation in the use of OCT imaging systems on typically large documents (up to 100x50 mm² for a biographical passport page). Yet, documents tend to present specific security markings in very distinct locations, which will be known to a trained investigator. One could address this issue by combining an OCT system with a wide field-of-view, multi-wavelength imaging device, one example being a video spectral comparator, with the resulting device providing correspondence between a wide field-of-view, colour image of the entire document provided by the video scan comparator and local, small field of view, depth-resolved volumes provided by the OCT scan head, targeting the security markings.

In terms of equipment cost, OCT imaging systems can range from \$10k [44] to upwards of \$50k, depending on the detection scheme, imaging speed and range, and scanning protocol, meaning that these systems are most suited for back-of-the-house forensic laboratories, and not necessarily for front-line use (in line with the typical use case of devices similar to, and including, the Foster and Freeman VSC). The VSC (and other surface-based complex imaging technologies) may be supported by the interferometric capabilities of OCT to investigate details which are below the surface of the document. Scanner-less systems are possible, such as those used in full-field OCT [45], where a 2-D camera is used as the detector.

The cost can be diminished even further if no scanning is needed, if the system in Figure 1 has its sample imaging system removed, and a fixed-direction, focused beam is directed to the sample, one would still retrieve a depth profile of the document under study, which may be sufficient to gauge whether the different layers have been tampered with.

In conclusion, manufacturers and issuing authorities are constantly playing catch-up from criminals involved in forgery of documents. We believe that the technology presented in this study can be used by multiple stakeholders in the field, namely the forensic scientists working to validate suspected forged documents in back-of-the-house laboratories, and the document manufacturers, having access to a non-destructive manner of quality control.

Effectively, a partnership between these stakeholders could culminate in the design of specific security features which can only be validated by means of the overarching principle of OCT imaging, low-coherence interferometry, with only relatively simple and low-cost technology necessary to check such features.

References

- [1] Passport fraud biggest threat to global security, INTERPOL chief warns in CNN interview, (n.d.). <https://www.interpol.int/en/News-and-Events/News/2010/Passport-fraud-biggest-threat-to-global-security-INTERPOL-chief-warns-in-CNN-interview> (accessed June 19, 2020).
- [2] Identification Document Validation Technology, GOV.UK. (n.d.). <https://www.gov.uk/government/publications/identity-document-validation-technology/identification-document-validation-technology> (accessed June 1, 2020).
- [3] S. Baechler, P. Margot, Understanding crime and fostering security using forensic science: The example of turning false identity documents into forensic intelligence, *Secur J.* 29 (2016) 618–639. <https://doi.org/10.1057/sj.2015.26>.
- [4] European Police Office, SOCTA 2013: EU Serious and Organised Crime Threat Assessment, 2013. <https://www.europol.europa.eu/activities-services/main-reports/eu-serious-and-organised-crime-threat-assessment-socta-2013>.
- [5] S. Baechler, O. Ribaux, P. Margot, 2012 Student Paper: Toward a Novel Forensic Intelligence Model: Systematic Profiling of False Identity Documents, *Forensic Science Policy & Management: An International Journal.* 3 (2012) 70–84. <https://doi.org/10.1080/19409044.2012.744120>.
- [6] European Police Office, OCTA 2009: EU Organised Crime Threat Assessment, 2009. <https://www.europol.europa.eu/activities-services/main-reports/octa-2009-eu-organised-crime-threat-assessment>.
- [7] S. Baechler, M. Morelato, O. Ribaux, A. Beavis, M. Tahtouh, K.P. Kirkbride, P. Esseiva, P. Margot, C. Roux, Forensic intelligence framework. Part II: Study of the main generic building blocks and challenges through the examples of illicit drugs and false identity documents monitoring, *Forensic Science International.* 250 (2015) 44–52. <https://doi.org/10.1016/j.forsciint.2015.02.021>.
- [8] Thales Group, Secure passport: Security & design (illustrated guide), (n.d.). <https://www.thalesgroup.com/en/markets/digital-identity-and-security/government/passport/passport-security-design> (accessed June 2, 2020).
- [9] S. Sugawara, Passport examination by a confocal-type laser profile microscope, *Forensic Sci.Int.* 178 (2008) 40–45. <https://doi.org/10.1016/j.forsciint.2008.02.004>.
- [10] J. Takalo, J. Timonen, J. Sampo, M. Rantala, S. Siltanen, M. Lassas, Using the fibre structure of paper to determine authenticity of the documents: Analysis of transmitted light images of stamps and banknotes, *Forensic Science International.* 244 (2014) 252–258. <https://doi.org/10.1016/j.forsciint.2014.09.002>.
- [11] Rafael Vieira, Mário Antunes, Catarina Silva, Ana Assis, Automatic Documents Counterfeit Classification Using Image Processing and Analysis, in: *Pattern Recognition and Image Analysis: 8th Iberian Conference, IbPRIA 2017, Faro, Portugal, June 20-23, 2017, Proceedings*, Springer International Publishing, Faro, Portugal, 2017. http://dx.doi.org/10.1007/978-3-319-58838-4_44.
- [12] D. Potolinca, I.C. Negru, V. Vasilache, C. Arsene, M. Paduraru, I. Sandu, Forensic Expertise of the Paper Support of Counterfeit Documents, *Mat.Plast.* 54 (2017) 186–185. <https://doi.org/10.37358/MP.17.1.4813>.
- [13] Document Examination, (n.d.). <http://www.fosterfreeman.com/2017-03-06-15-40-12/document-examination.html> (accessed June 19, 2020).
- [14] National Forensic Science Technology Center, *Forensic Science Simplified*, (2013). <http://www.forensicssciencesimplified.org/docs/> (accessed June 10, 2020).
- [15] D. Huang, E.A. Swanson, C.P. Lin, J.S. Schuman, W.G. Stinson, W. Chang, M.R. Hee, T. Flotte, K. Gregory, C.A. Puliafito, A. Et, Optical coherence tomography, *Science.* 254 (1991) 1178–1181. <https://doi.org/10.1126/science.1957169>.
- [16] M. Nioi, P.E. Napoli, S.M. Mayerson, M. Fossarello, E. d’Aloja, Optical coherence tomography in forensic sciences: a review of the literature, *Forensic Sci Med Pathol.* 15 (2019) 445–452. <https://doi.org/10.1007/s12024-019-00136-z>.
- [17] A.G. Podoleanu, Optical coherence tomography, *Journal of Microscopy.* 247 (2012) 209–219. <https://doi.org/10.1111/j.1365-2818.2012.03619.x>.

- [18] N. Laan, R.H. Bremmer, M.C.G. Aalders, K.G. de Bruin, Volume Determination of Fresh and Dried Bloodstains by Means of Optical Coherence Tomography, *Journal of Forensic Sciences*. 59 (2014) 34–41. <https://doi.org/10.1111/1556-4029.12272>.
- [19] M.J.M. Marques, J. Pomeroy, R. Green, C. Deter, A. Bradu, A. Podoleanu, Improved visualization of decomposing tattoos using optical coherence tomography, in: S.A. Boppart, M. Wojtkowski, W.-Y. Oh (Eds.), *Optical Coherence Imaging Techniques and Imaging in Scattering Media III*, SPIE, Munich, Germany, 2019: p. 63. <https://doi.org/10.1117/12.2526757>.
- [20] W.-J. Choi, G.-H. Min, B.-H. Lee, J.-H. Eom, J.-W. Kim, Counterfeit Detection Using Characterization of Safety Feature on Banknote with Full-field Optical Coherence Tomography, *J. Opt. Soc. Korea*, JOSK. 14 (2010) 316–320.
- [21] N. Zhang, C. Wang, Z. Sun, H. Mei, W. Huang, L. Xu, L. Xie, J. Guo, Y. Yan, Z. Li, X. Xu, P. Xue, N. Liu, Characterization of automotive paint by optical coherence tomography, *Forensic Science International*. 266 (2016) 239–244. <https://doi.org/10.1016/j.forsciint.2016.06.007>.
- [22] C. Wang, N. Zhang, Z. Sun, Z. Li, Z. Li, X. Xu, Recovering hidden sub-layers of repainted automotive paint by 3D optical coherence tomography, *Australian Journal of Forensic Sciences*. 51 (2019) 331–339. <https://doi.org/10.1080/00450618.2017.1367418>.
- [23] S. Hwang, H. Song, S.-W. Cho, C.E. Kim, C.-S. Kim, K. Kim, Optical measurements of paintings and the creation of an artwork database for authenticity, *PLOS ONE*. 12 (2017) e0171354. <https://doi.org/10.1371/journal.pone.0171354>.
- [24] R. Khutlang, F.V. Nelwamondo, A. Singh, Segmentation of Forensic Latent Fingerprint Images Lifted Contact-Less from Planar Surfaces with Optical Coherence Tomography, in: 2015 IEEE 39th Annual Computer Software and Applications Conference, 2015: pp. 30–34. <https://doi.org/10.1109/COMPSAC.2015.166>.
- [25] N. Zhang, C. Wang, Z. Sun, Z. Li, L. Xie, Y. Yan, L. Xu, J. Guo, W. Huang, Z. Li, J. Xue, H. Liu, X. Xu, Detection of latent fingerprint hidden beneath adhesive tape by optical coherence tomography, *Forensic Science International*. 287 (2018) 81–87. <https://doi.org/10.1016/j.forsciint.2018.03.030>.
- [26] M. Leich, S. Kiltz, J. Dittmann, C. Vielhauer, Non-destructive forensic latent fingerprint acquisition with chromatic white light sensors, in: *Media Watermarking, Security, and Forensics III*, International Society for Optics and Photonics, 2011: p. 78800S. <https://doi.org/10.1117/12.872331>.
- [27] S.K. Dubey, T. Anna, C. Shakher, D.S. Mehta, Fingerprint detection using full-field swept-source optical coherence tomography, *Appl. Phys. Lett.* 91 (2007) 181106. <https://doi.org/10.1063/1.2800823>.
- [28] A. Zam, R. Dsouza, H.M. Subhash, M.-L. O'Connell, J. Enfield, K. Larin, M.J. Leahy, Feasibility of correlation mapping optical coherence tomography (cmOCT) for anti-spoof sub-surface fingerprinting, *Journal of Biophotonics*. 6 (2013) 663–667. <https://doi.org/10.1002/jbio.201200231>.
- [29] M.-R. Nasiri-Avanaki, A. Meadway, A. Bradu, R.M. Khoshki, A. Hojjatoleslami, A.Gh. Podoleanu, Anti-Spoof Reliable Biometry of Fingerprints Using En-Face Optical Coherence Tomography, *OPJ*. 01 (2011) 91–96. <https://doi.org/10.4236/opj.2011.13015>.
- [30] M.J. Marques, S. Rivet, A. Bradu, A. Podoleanu, Complex master-slave for long axial range swept-source optical coherence tomography, *OSA Continuum*. 1 (2018) 1251. <https://doi.org/10.1364/OSAC.1.001251>.
- [31] R. Leitgeb, C. Hitzenberger, A. Fercher, Performance of fourier domain vs time domain optical coherence tomography, *Optics Express*. 11 (2003) 889. <https://doi.org/10.1364/OE.11.000889>.
- [32] X. Attendu, R.M. Ruis, Simple and robust calibration procedure for k-linearization and dispersion compensation in optical coherence tomography, *J. Biomed. Opt.* 24 (2019) 1. <https://doi.org/10.1117/1.JBO.24.5.056001>.

- [33] C. Photiou, C. Pitris, Comparison of tissue dispersion measurement techniques based on optical coherence tomography, *J. Biomed. Opt.* 24 (2019) 1. <https://doi.org/10.1117/1.JBO.24.4.046003>.
- [34] A.Gh. Podoleanu, A. Bradu, Master–slave interferometry for parallel spectral domain interferometry sensing and versatile 3D optical coherence tomography, *Optics Express*. 21 (2013) 19324. <https://doi.org/10.1364/OE.21.019324>.
- [35] S. Rivet, M. Maria, A. Bradu, T. Feuchter, L. Leick, A. Podoleanu, Complex master slave interferometry, *Optics Express*. 24 (2016) 2885. <https://doi.org/10.1364/OE.24.002885>.
- [36] Documentos de Identificação - Documentos de Segurança - INCM, (n.d.). https://www.incm.pt/portal/gs_docid.jsp?lang=en (accessed June 9, 2020).
- [37] A. Bradu, L. Ma, J.W. Bloor, A. Podoleanu, Dual optical coherence tomography/fluorescence microscopy for monitoring of *Drosophila melanogaster* larval heart, *J. Biophoton*. 2 (2009) 380–388. <https://doi.org/10.1002/jbio.200910021>.
- [38] M. Bondu, M.J. Marques, P.M. Moselund, G. Lall, A. Bradu, A. Podoleanu, Multispectral photoacoustic microscopy and optical coherence tomography using a single supercontinuum source, *Photoacoustics*. 9 (2018) 21–30. <https://doi.org/10.1016/j.pacs.2017.11.002>.
- [39] G. Nteroli, M. Bondu, P.M. Moselund, A. Podoleanu, A. Bradu, Developments on using supercontinuum sources for high resolution multi-imaging instruments for biomedical applications, in: *Opto-Acoustic Methods and Applications in Biophotonics IV*, International Society for Optics and Photonics, 2019: p. 110770N. <https://doi.org/10.1117/12.2527111>.
- [40] N.M. Israelsen, C.R. Petersen, A. Barh, D. Jain, M. Jensen, G. Hanneschläger, P. Tidemand-Lichtenberg, C. Pedersen, A. Podoleanu, O. Bang, Real-time high-resolution mid-infrared optical coherence tomography, *Light: Science & Applications*. 8 (2019) 11. <https://doi.org/10.1038/s41377-019-0122-5>.
- [41] I. Zorin, J. Kilgus, R. Su, B. Lendl, M. Brandstetter, B. Heise, Multimodal mid-infrared optical coherence tomography and spectroscopy for non-destructive testing and art diagnosis, in: P. Targowski, R. Groves, H. Liang (Eds.), *Optics for Arts, Architecture, and Archaeology VII*, SPIE, Munich, Germany, 2019: p. 22. <https://doi.org/10.1117/12.2528279>.
- [42] H. Momiyama, Y. Sasaki, I. Yoshimine, S. Nagano, T. Yuasa, C. Otani, Improvement of the depth resolution of swept-source THz-OCT for non-destructive inspection, *Opt. Express*. 28 (2020) 12279. <https://doi.org/10.1364/OE.386680>.
- [43] Regulation (EU) 2019/1157 of the European Parliament and of the Council of 20 June 2019 on strengthening the security of identity cards of Union citizens and of residence documents issued to Union citizens and their family members exercising their right of free movement (Text with EEA relevance.), 2019. <http://data.europa.eu/eli/reg/2019/1157/oj/eng> (accessed June 22, 2020).
- [44] S. Kim, M. Crose, W.J. Eldridge, B. Cox, W.J. Brown, A. Wax, Design and implementation of a low-cost, portable OCT system, *Biomed. Opt. Express*, BOE. 9 (2018) 1232–1243. <https://doi.org/10.1364/BOE.9.001232>.
- [45] A. Dubois, L. Vabre, A.-C. Boccara, E. Beaufrepaire, High-resolution full-field optical coherence tomography with a Linnik microscope, *Appl. Opt.*, AO. 41 (2002) 805–812. <https://doi.org/10.1364/AO.41.000805>.

Highlights

- Need to distinguish legitimate from counterfeit documents.
- High-throughput, sensitive, high-resolution imaging methods required.
- Modern documents present sub-surface security features.
- Optical coherence tomography (OCT) allows sub-surface, non-destructive imaging.
- OCT was used here to image security features embedded in questioned documents.

Journal Pre-proofs